Dalton Transactions

ROYAL SOCIETY OF CHEMISTRY

PAPER

View Article Online
View Journal | View Issue

Cite this: *Dalton Trans.*, 2026, **55**, 196

Constructing a crosslinked architecture in conjugated microporous polymers for highly efficient uranium(VI) photoreduction

Guangyu Xu,[a,b] Qi Chen,[c] Caijuan Lu,[d] Luxin Huang,[d] Zhengfeng Hu*[e] and Muqing Qiu *[a]

Received 21st October 2025,
Accepted 27th November 2025

DOI: 10.1039/d5dt02520f

rsc.li/dalton

Herein, the exploration of advanced materials in the highly effective removal of uranium is highly desired. Three amidoxime-functionalized conjugated microporous polymer (CMP-AO) networks with different architectures were synthesized by the Sonogashira–Hagihara coupling reaction. The effect of various factors on the photoreduction of U(VI) on CMP-AO was systemically investigated. The fast photocatalytic efficiency (K_1 = 0.00713 min^{-1}), superior selectivity and prominent recyclability of U(VI) on CMPs1-AO was achieved due to the outstanding separation of photogenerated carriers, good chemical stability, and massive functional groups. According to trapping and EPR analysis, the photogenerated electrons and superoxide radicals played an important role in U(VI) photoreduction. The introduction of AO groups was shown to be favorable for the photoreduction of U(VI) into U(VI) by XPS analysis. These findings are crucial for the rational design of CMPs in removing U(VI) from aqueous solutions.

1. Introduction

The consumption of fossil fuels has facilitated the process of industrialization and urbanization over the past few decades. The rapid development of nuclear power effectively alleviated the shortage of fossil energy and the environmental pollution, and it was regarded as a clean energy route to achieve carbon neutrality.[1] However, various radionuclides will inevitably be discharged into the environment during the exploitation of the U(VI) ore, post-process of spent fuel and accidents of nuclear power plants, demonstrating the severe effects on the environment and human health due to its radioactivity and high toxicity.[2] Therefore, the highly efficient removal of uranium is of great importance for the sustainable development of nuclear energy.[3]

In particular, the development of advanced materials with high removal capacity is desired. In the past decades, numerous novel nanomaterials (*e.g.*, graphene oxides,[4–6] metal organic frameworks (MOFs),[7–9] covalent organic frameworks (COFs),[10–13] and conjugated microporous polymers (CMPs)[14–18]) have been widely utilized for the removal of U(VI) from aqueous solutions. Among these novel nanomaterials, CMPs as typical novel nanoparticles can be fabricated by combining an extended π-conjugation with a permanently microporous skeleton.[19,20] For instance, the highly efficient photoreduction of U(VI) on CMP (99.5% within 2 h) achieved by harnessing sunlight was very appealing due to the tunable porosity, high crystallinity and excellent charge separation of CMP.[21] The light-driven catalysis-assisted U(VI) reduction into U(IV) is regarded as an effective strategy to remove U(VI) from aqueous solutions due to the large difference of solubility between U(VI) and U(IV).[22] Nevertheless, the application of CMPs is severely hindered in actual environmental cleanup due to the high cost of the monomer, limited active sites, and poor stability of CMPs under harsh conditions (*e.g.*, high salinity and presence of strong bases/acids). The synthesis of stable CMP materials with high removal capacity, low cost and easy preparation still remains challenging.

The objectives of this study are as follows: (1) to synthesize CMP-AO using polymerization and amidoximation methods and characterize it using microscopic (*e.g.*, SEM, XRD, FTIR, and XPS) and optical techniques (*e.g.*, DRS, PL, TPC, and EIS); (2) to investigate the effect of different factors (*e.g.*, reaction time, pH, and competitive ions) on U(VI) photoreduction by CMP-AO; and (3) to demonstrate the photoreduction mechanism of U(VI) on CMP-AO using trapping, XPS and EPR analysis. The highlight of this study is the actual application of

[a]*School of Life and Environmental Sciences, Shaoxing University, Shaoxing 312000, PR China. E-mail: qiumuqing@usx.edu.cn*
[b]*School of Earth and Environmental Sciences, The University of Queensland, St Lucia, QLD 4072, Australia*
[c]*Shaoxing Ecological and Environmental Monitoring Center of Zhejiang Province, Shaoxing 312000, PR China*
[d]*Shaoxing Jiangxianghe Agricultural Development Co., Ltd, Shaoxing 312000, PR China*
[e]*Key Laboratory of Environmental Pollution Control Technology Research of Zhejiang Province, Ecological and Environmental Science and Research Institute of Zhejiang Province, Hangzhou, Zhejiang 310007, PR China. E-mail: 57276606@qq.com*

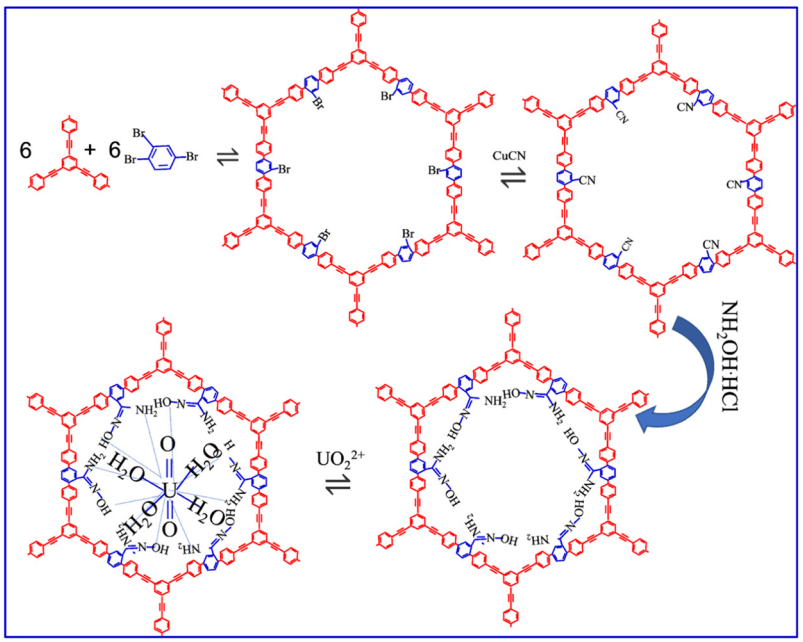

Scheme 1 Synthesis of CMP-AO and the adsorption mechanism of U(VI) on CMP-AO.

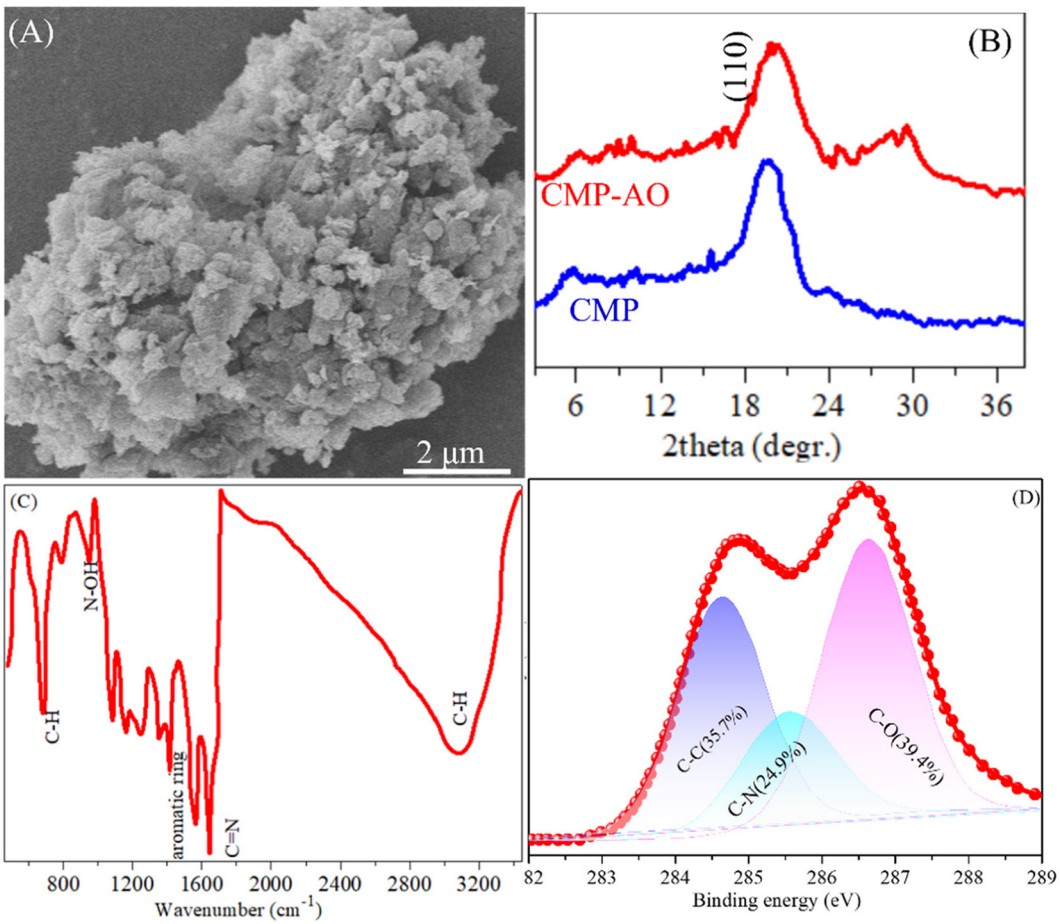

Fig. 1 Characterization of CMP-AO: (A and B) SEM and XRD, respectively, and (C and D) FTIR and C 1s XPS spectra, respectively.

CMP-AO towards various radionuclides from aqueous solutions.

2. Experimental section

2.1 Materials and methods

1,3,5-Triethynylbenzene (TEB), 1,2,4-tribromobenzene (TBB), triethylamine (Et_3N), and hydroxylamine hydrochloride ($NH_2OH{\cdot}HCl$) of analytical grade were purchased from Sinopharm Chemical Reagent Co., Ltd. The other chemicals (*e.g.*, toluene, tetrakis-(triphenylphosphine)palladium(0), copper (I) iodide, acetone, (diacetoxyiodo)benzene ($PhI(OAc)_2$), dichloroethane, malononitrile ($C_3H_2N_2$), $K_3Fe(CN)_6$, $NaHCO_3$, *p*-BQ, TBA, EDTA-Na and KI) of analytic grade were obtained from Aladdin Biochemistry Chemical Reagent Co., Ltd (Shanghai, China). U(VI) stock solutions (0.1 mol L^{-1}) were prepared by dissolving $UO_2(NO_3)_2{\cdot}6H_2O$ (analytic reagent, as a gift from Hubei Chushengwei Co., Ltd) into DI water in a glove box.

2.2 Synthesis and characterization of CMP-AO

CMP-AO was synthesized by cross-coupling chemistry of TBB with TEB in a mixture of toluene and Et_3N solution.[23,24] Briefly, the monomer of TEB and coupling agent of TBB were placed into a mixture of toluene and Et_3N, and then heated at 80 °C for 3 days under tetrakis-(triphenylphosphine)palladium (0), copper(I) iodide in a N_2 atmosphere. Then, malononitrile was added into two intermediates to generate cyano groups under $Ph(OAc)_2$ and dichloroethane conditions. Then, the as-prepared intermediates were functionalized by $NH_2OH{\cdot}HCl$ under Et_3N condition to convert the cyano group into AO groups (Scheme 1). CMP, CMP1-AO and CMP2-AO refer to the mass fractions of the AO group with 0, 1 and 2 wt%, respectively. The detailed synthesis processes are provided in the SI.

The as-prepared CMP-AO was characterized by scanning electron micrometer (SEM, Oxford X-max micrometers), X-ray diffraction (XRD, Rigaku SmartLab SE X-ray diffractometer), Fourier transform infrared (FT-IR, Bruker Vertex70 spectrometer), X-ray photoelectron spectrometers (XPS, Theta probe), BET surface area and porosity analyzer (JT-2000, Haixinrui Technology, Beijing). The optical properties of CMP-AO were determined using photoluminescence (PL, ELS1000-Edinburgh Instruments), UV-vis diffuse reflectance spectra (DRS, Shimadzu UV-2700 spectrophotometer), electron paramagnetic resonance (EPR, Bruker EPR A300 spectrometer), transient photocurrent response (TPR, TranPVC 900, Oriental Spectra), and electrochemical impedance spectroscopy (EIS, VersaScan, Ametek Scientific Instruments).

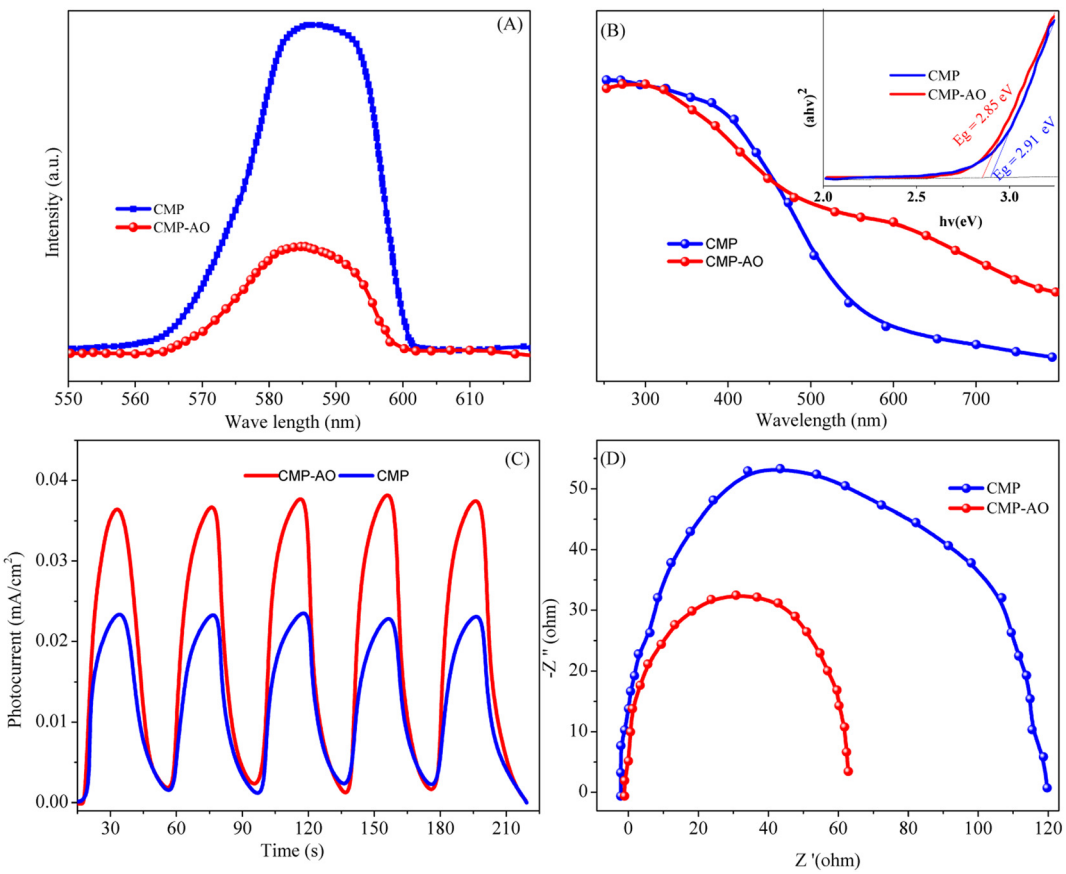

Fig. 2 The electrochemical properties of CMP-AO: (A and B) PL and DRS, respectively, inset shows the plot of $(\alpha h\nu)^2$ *vs.* $h\nu$. (C and D) TPC and NIS, respectively.

2.3 Removal experiments

All batch experiments as a function of various factors (*i.e.*, time, pH, catalysts, competitive cations) were conducted in a photoreactor under visible light irradiation (300 W xenon lamp with a 420 nm cut-off filter) under ambient conditions. Briefly, 10.0 mg photocatalyst was added into 50 mL 10 mg L^{-1} U(VI) solution. After allowing the reaction to proceed under dark conditions for 60 min, the dispersion was irradiated at different time intervals. The pH of the solution was adjusted by using 0.1–1.0 mol L^{-1} HCl/NaOH. To assess the reusability, regeneration experiments of U(VI) on CMP-AO were conducted by collecting CMP-AO after the reaction and then pouring it into $NaHCO_3$ (10 mL, 0.1 mol L^{-1}) under vigorous stirring for 30 min. After that, CMP-AO was washed by DI water and dried at 120 °C overnight for next use. The trapping experiments were investigated by adding 5 mL of various scavengers (*e.g.*, *p*-benzoquinone (*p*-BQ, 1 mmol L^{-1}), *tert* butyl alcohol (TBA, 1 mmol L^{-1}), EDTA-Na (1 mmol L^{-1}) and KI (1 mmol L^{-1}) to eliminate the superoxide ($^{\bullet}O_2^-$), hydroxyl ($^{\bullet}OH$), electron (e^-) and hole (h^+) radicals, respectively) into 10.0 mg CMP2-AO and 45 mL 10 mg L^{-1} U(VI) solution. After adsorption equilibrium under dark condition for 60 min, the dispersion was irradiated under visible light for 360 min. After the reaction, aliquots of the dispersion were separated from the liquid phase by 0.22 μm syringe filter. The concentration of U(VI) in aqueous phase was measured by UV-Vis spectrophotometer (Arsenazo III as color agent) at 650 nm.

3. Results and discussion

3.1 Characterization

The morphologies and mineralogy of CMP-AO were verified by SEM (Fig. 1A) and XRD (Fig. 1B), respectively. The stacking fibers with a thickness of a few micrometers matched well with the previous reported.[21] The wide XRD peaks showed the typical characteristic of amorphous CMPs, whereas the strong diffraction peaks at 2θ of 20.7° were assigned to the (110)

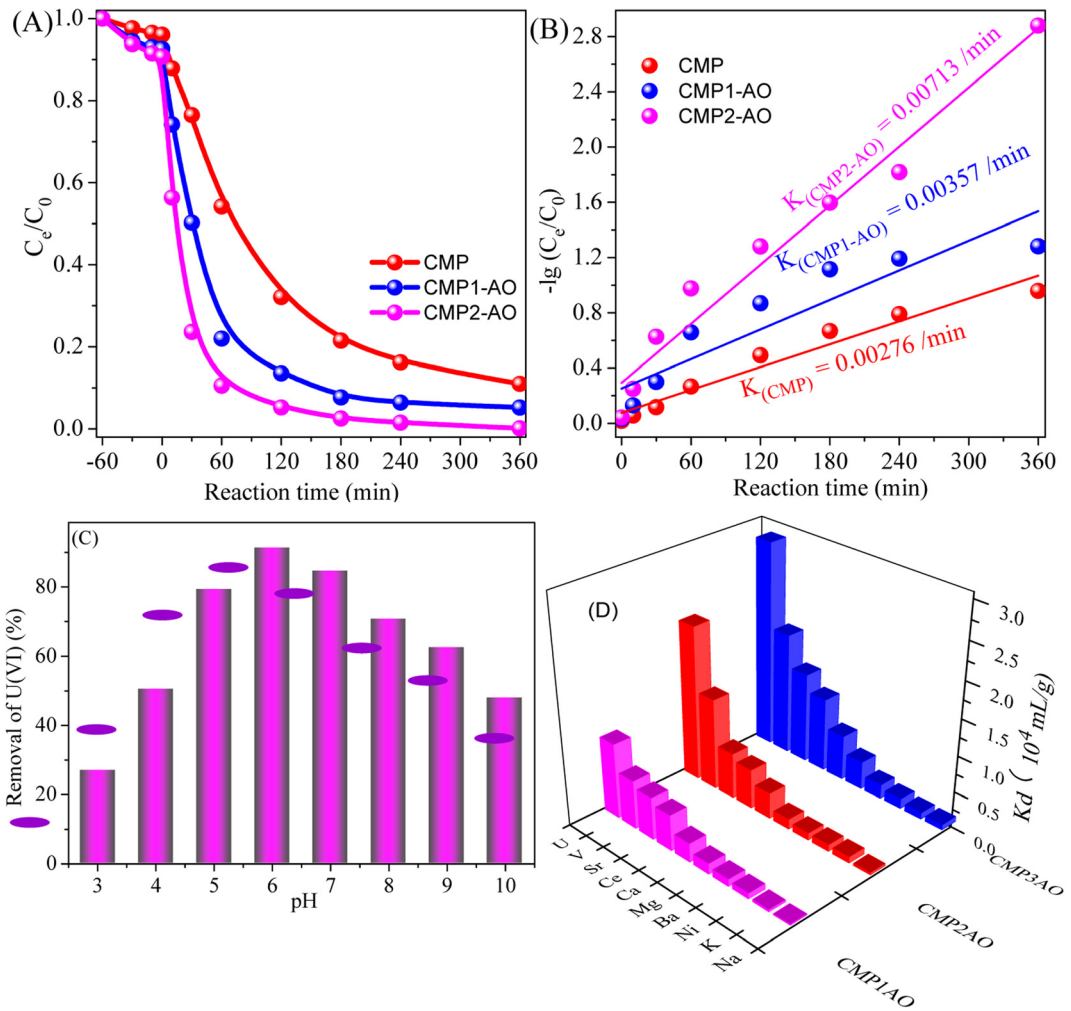

Fig. 3 The effect of the photocatalysts (A) and fitting of the pseudo-first-order kinetic model (B), pH (C) and competitive cations (D) on the U(VI) photoreduction on CMP-AO.

plane of CMP-AO.[19] In addition, no change of XRD spectra under different harsh conditions (*e.g.*, immersing in pH 2 of HCl and pH 12 of NaOH for 24 h) manifested the chemical stability of CMP-AO. The successful amidoximation and polymerization of CMPs were confirmed by FT-IR spectra (Fig. 1C). The characteristic peaks at 1300–1600 (*e.g.*, ~1350, 1413 and 1567 cm^{-1}) and 650–800 cm^{-1} (*e.g.*, ~679, 787 cm^{-1}) indicated the skeletal vibration and C–H bending vibration of the aromatic ring of CMP, respectively.[21,25] The absence of C≡N (2220 cm^{-1}) and the appearance of C=N (1645 cm^{-1}) and N–OH (954 cm^{-1}) of the AO groups showed the valid graft of the amidoxime groups.[26] The absorption peaks at 3105 cm^{-1} could be assigned to the stretching vibration of the aromatic C–H groups.[27] As shown in Fig. 1D, the C 1s high-resolution spectra of CMPs can be deconvoluted into three peaks at 284.6, 285.4 and 286.2 eV, corresponding to C–C, C–O and C=N/C=O, respectively.[28] Compared to CMP (Fig. S1A), the weight loss of CMP-AO was slightly decreased at 300–400 °C due to the degradation of AO. As shown by the N_2 adsorption–desorption curve (Fig. S1B), the type-IV isotherms (hysteresis at relative pressure of 0.8–1.0) demonstrated the coexistence of mesopores and macropores in CMP. The BET specific surface area (830 m^2 g^{-1}) and total pore volumes (1.25 m^3 g^{-1}) of CMP-AO were higher than CMP (419 m^2 g^{-1} and 0.53 m^3 g^{-1}), which was more favorable for U(VI) adsorption. The structural characterization of CMP2-AO was conducted *via* solid-state ^{13}C NMR at the molecular level (Fig. S2A). The prominent signal peaks at δ = 123.3 and 131.1 ppm corresponded to C–H and C–C≡C– structure, respectively. In addition, the signal peak at δ = 89.1 ppm further demonstrated the synthesis of CMP-AO.[29] These characterizations concluded that CMPs-AO exhibited beneficial properties with its easy processing, low cost, and chemical/thermal stability.

Fig. 2A, B, C and D show the PL, DRS, TPC and NIS spectra of CMP-AO, respectively. Compared to CMP (high emission peak at 580–590 nm, Fig. 2A), the significant decrease of the PL intensity indicated the low recombination of the electron–hole pairs of CMP-AO.[30] Therefore, the introduction of AO groups was beneficial to the separation of the photo-generated charges.[31] Apart from the broad absorption intensity at 200–300 nm (Fig. 2B), the enhanced relative intensity of CMP-AO at wavelengths >500 nm showed the extended adsorption range from UV to visible region.[32] According to the calculation of the Tauc plots (inset in Fig. 2B), the optical bandgaps of CMP-AO (~2.85 eV) were slightly lower than those of CMP

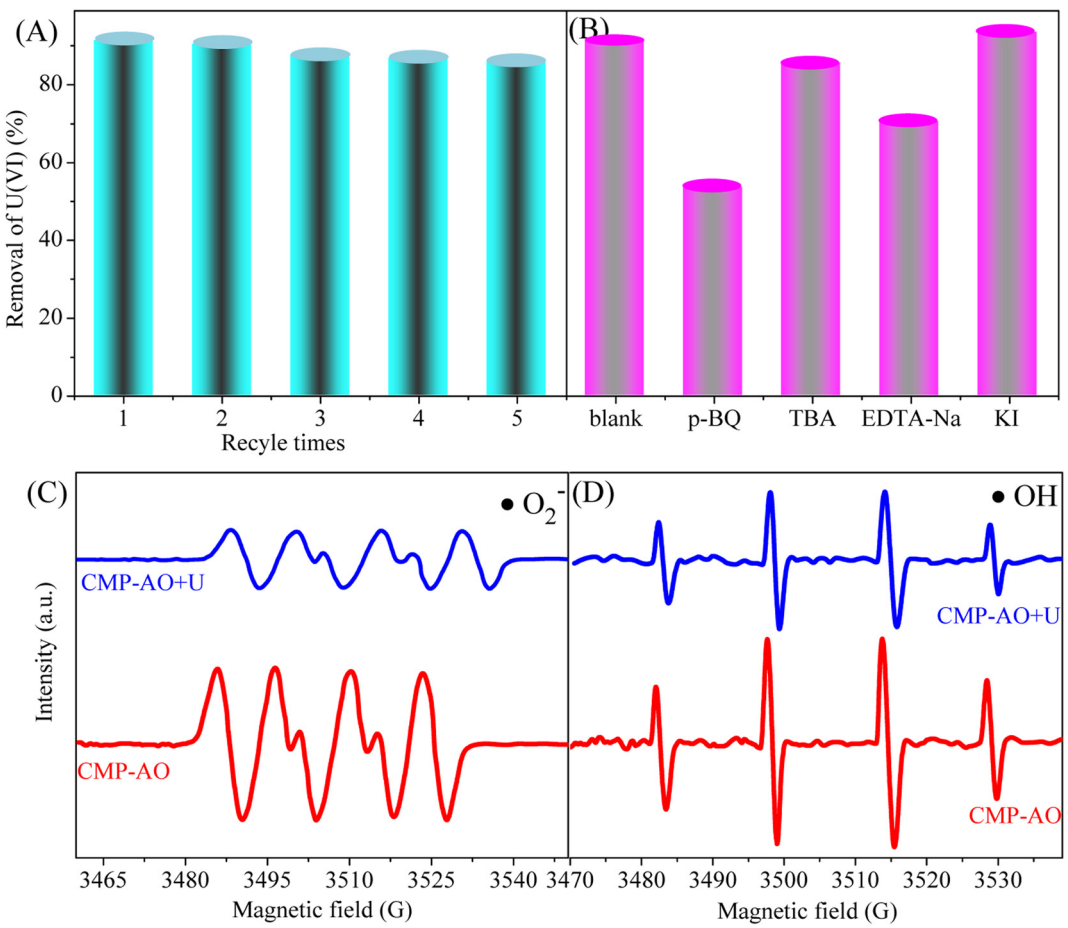

Fig. 4 The regeneration (A) and trapping (B) of U(VI) on CMP-AO. (C and D): EPR spectra of $^{\bullet}O_2^-$ and $^{\bullet}OH$ radicals, respectively.

(~2.91 eV), indicating the superior photocatalytic performance of CMP-AO.[19] The high photocurrent response (Fig. 2C) further demonstrated the excellent separation efficiency of photogenerated carriers of CMP-AO.[33] According to EIS Nyquist analysis (Fig. 2D), the low arc radius of CMP-AO indicated the high electron transfer of electrons.[34] Based on the electrochemical characterizations, the unique structures of CMP-AO can effectively hinder the recombination of photogenerated electron–hole pairs and extend the absorption range from UV to visible light, resulting in the highly effective photocatalytic activity.

3.2 Evaluation of the photocatalytic performance

The effect of various factors (*e.g.*, photocatalyst, pH, reaction time, competitive cations) on U(VI) removal was investigated to evaluate the photocatalytic performance of CMPs-AO. The photocatalytic performance of CMP2-AO (90% within 60 min under visible light irradiation, Fig. 3A) was two times higher than that of CMP (~45%) due to the highly efficient selectivity of AO groups towards U(VI). Compared to CMP (K_1 = 0.00276 min^{-1}, Fig. 3B) and CMP1-AO (K_1 = 0.00357 min^{-1}), the high rate constants of CMP2-AO (K_1 = 0.00713 min^{-1}) further demonstrated the superior photocatalytic performance of CMP-AO due to the fast transfer of multiple electrons.[35]

The removal kinetics of U(VI) on CMP, CMP1-AO and CMP2-AO can be satisfactorily fitted by pseudo-second order kinetic model according to the high correlation coefficient (R^2 > 0.98, Fig. S2B and Table S1), indicating the chemosorption of U(VI) on CMP-AO. Generally, the pH value of the aqueous solution influenced the speciation of U(VI) and determined the surface charge of CMP-AO. The removal of U(VI) on CMP2-AO gradually increased with increasing pH. The highest removal was observed at pH 6.0 (Fig. 3C, 92%), whereas the U(VI) removal decreased with further increase of pH above 6.0. The increased removal at pH 2.0–6.0 could be attributed to the electrostatic attraction of the positive U(VI) species (*e.g.*, UO_2^{2+}, $UO_2(OH)^+$ and $(UO_2)_3(OH)_5^+$, Fig. S3A) and the negative charge of CMPs-AO (negative charge at pH > 5 by zeta potential in Fig. S3B).[22] The decreased removal of U(VI) at pH > 7.0 was also attributed to the electrostatic repulsion of the negatively charged U(VI) (*e.g.*, $UO_2(CO_3)_2^{2-}$/$UO_2(CO_3)_3^{4-}$, Fig. S3A) and negative charge of CMP-AO. By comparison, the amidoximation process endowed CMP1 with selectivity towards U(VI). Considering the actual applications, a comparison of the U(VI) removal with other heavy metals (Na, K, Ni, Ba, Mg, Ca, Ce, Sr, V) is shown in Fig. 3D. The distribution coefficient (K_d, 2.85 × 10^4 mL g^{-1}) of U(VI) on CMP2-AO was significantly higher than that for the other heavy metals (*e.g.*, 0.075 × 10^4 mL g^{-1} of Na, 0.14 2.85 × 10^4 mL g^{-1} of Ni, 1.25 2.85 × 10^4 mL g^{-1} of Sr and 1.69 2.85 × 10^4 mL g^{-1} of V). The exclusive U(VI) removal on CMP-AO could be attributed to the high selectivity of AO towards U(VI). The chemical stability of CMP-AO was also evaluated by the generation experiments. As shown in Fig. 4A, the slight decrease of the U(VI) removal after five cycles revealed the potential application of CMP-AO in actual U(VI) remediation. These findings demonstrated that CMP-AO exhibited the fast removal efficiency, high selective enrichment and excellent chemical stability towards U(VI) in aqueous solutions.

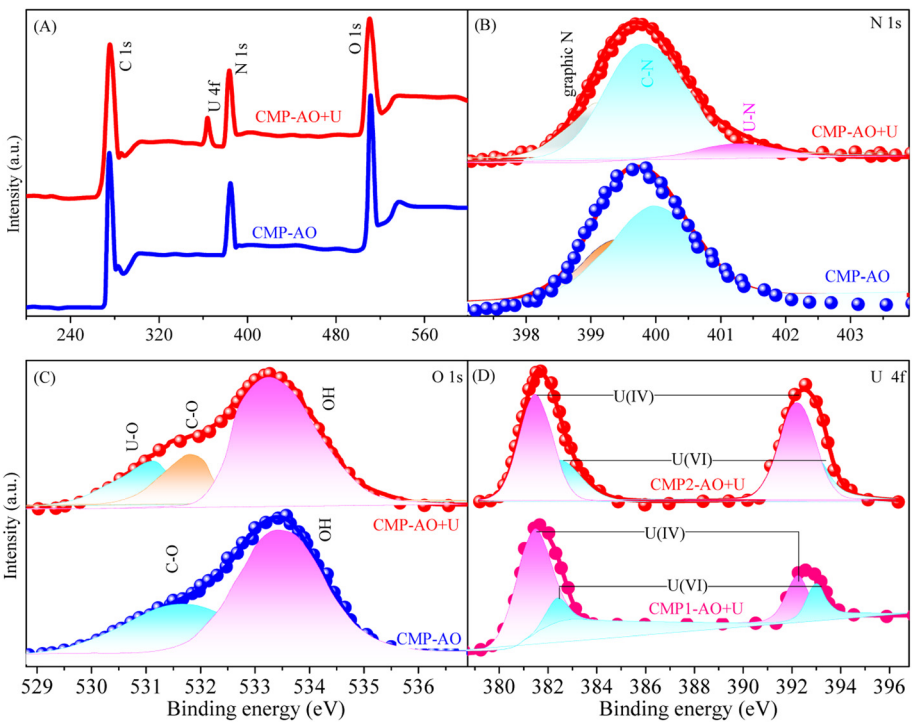

Fig. 5 XPS analysis of CMP-AO before and after U(VI) reaction: (A and B) total scan survey and high-resolution N 1s spectra, respectively, and (C and D) high-resolution O 1s and U 4f spectra, respectively.

3.3 Interaction mechanism

The interaction mechanism of U(VI) photoreduction on CMP-AO was characterized using trapping, EPR and XPS analysis. The generation of the active species during photocatalysis was determined by trapping experiments (Fig. 4B) and EPR spectra (Fig. 4C and D). After adding *p*-BQ and EDTA-Na, the significant inhibition of the CMP-AO photocatalytic activity reflected that $^{\bullet}O_2^-$ and e^- were key active species towards the photoreduction of U(VI).[12] Compared to the original CMP-AO, the decrease of the strong consecutive $^{\bullet}O_2^-$ peaks after U(VI) reaction indicated the rapid consumption of $^{\bullet}O_2^-$ radicals during U(VI) photoreduction.[36] However, there was no significant change in the $^{\bullet}OH$ signal of CMP-AO before and after the U(VI) reaction, indicating that the U(VI) photoreduction was not dependent on the $^{\bullet}OH$ radicals. The trapping and EPR analysis indicated that the effective photoreduction of U(VI) was attributed to the $^{\bullet}O_2^-$ radicals and e^-.

Fig. 5 shows the XPS analysis of CMP-AO after and before the U(VI) reaction. Apart from the main C 1s, N 1s and O 1s (Fig. 5A), the presence of U 4f with the decreased intensity of O 1s indicated that the U(VI) photoreduction was related to the oxygen-containing functional groups.[5] The high-resolution N 1s XPS spectra of the original CMP-AO can be deconvoluted into graphic N (399.3 eV) and C–N (400.1 eV, Fig. 5B), whereas the new peaks at 401.5 eV of CMP-AO after the U(VI) reaction could be attributed to the U–N bonds.[7,37] Apart from the C–O (531.5 eV, Fig. 5C) and HO groups (533.5 eV), the presence of O–U groups (530.4 eV) demonstrated that the oxygen-containing functional groups played an important role in U(VI) photoreduction.[31,38] Compared to CMP, the enhanced intensity of the U 4f peaks (*i.e.*, U $4f_{7/2}$ and U $4f_{5/2}$ at 381.9 and 392.5 eV, respectively) indicated the high adsorption capacity of CMP-AO towards U(VI) due to the introduction of the AO groups. In addition, the U 4f peaks of both CMP1-AO and CMP2-AO can be deconvoluted into U(IV) (381.5 and 392.0 eV) and U(VI) species (382.2 and 393 eV).[24,32] XPS analysis indicated the photoreduction of U(VI) into U(VI) by CMP and CMP-AO under visible light irradiation.[39] Therefore, the interaction mechanism of U(VI) on CMP-AO included the electrostatic interaction, strong inner-sphere surface complexation and photoreduction of the adsorbed U(VI) into U(IV).

4. Conclusions

In summary, a CMP-AO with well-defined structure and massive functional groups was successfully fabricated through the polymerization and amidoximation methods. Noticeably, the unique merits of CMP-AO greatly improved the transport and separation of photogenerated charges, consequently resulting in outstanding photocatalytic performance (as high as 90% at visible-light irradiation of 60 min, two times higher than in CMP). In addition, CMP-AO exhibited excellent chemical stability and highly selective enrichment towards U(VI) due to the introduction of AO groups by XPS analysis. Superoxide radicals and photogenerated electrons played an important role in U(VI) photoreduction, as shown by trapping and EPR analysis. By virtue of the experimental and characterization results, the elaborate design of the desirable materials was an effective strategy for the highly effective removal of uranium in the actual environmental remediation.

Conflicts of interest

There are no conflicts to declare.

Data availability

All data supporting the findings of this study are included within the published article and its supplementary information (SI). Supplementary information of characterization, adsorption kinetics, the distribution of distribution of U(VI) speciation and the zeta potential are available. See DOI: https://doi.org/10.1039/d5dt02520f.

Acknowledgements

This work was supported by the Science and Technology Plan Project of Shaoxing (2024001020).

References

1 D. Tong, Q. Zhang, Y. Zheng, K. Caldeira, C. Shearer, C. Hong, Y. Qin and S. J. Davis, Committed emissions from existing energy infrastructure jeopardize 1.5 degrees C climate target, *Nature*, 2019, **572**, 373–377.
2 A. Cho, NUCLEAR SECURITY US planning test reactor to run on weapons-grade uranium, *Science*, 2023, **380**, 783–783.
3 M. Keener, C. Hunt, T. G. Carroll, V. Kampel, R. Dobrovetsky, T. W. Hayton and G. Menard, Redox-switchable carboranes for uranium capture and release, *Nature*, 2020, **577**, 652–655.
4 L. Ke, P. Li, X. Wu, S. Jiang, M. Luo, Y. Liu, Z. Le, C. Sun and S. Song, Graphene-like sulfur-doped g-C_3N_4 for photocatalytic reduction elimination of UO_2^{2+} under visible Light, *Appl. Environ. Biotechnol.*, 2017, **205**, 319–326.
5 W. Zhang, B. Wang, H. Cui, Q. Wan, B. Yi and H. Yang, Unveiling the exciton dissociation dynamics steered by built-in electric fields in conjugated microporous polymers for photoreduction of uranium(VI) from seawater, *J. Colloid Interface Sci.*, 2024, **662**, 377–390.
6 W. Zhang, X. Luo, L. Liu, M. Lei, Q. Wan, B. Yi, F. Yu and H. Yang, Engineering exciton dissociation and intermolecular charge transfer to boost superoxide radical in conjugated microporous polymers for simultaneous elimination of coexisting contaminants, *Chem. Eng. J.*, 2024, **499**, 156552.
7 X. Liu, Z.-H. Peng, L. Lei, R.-X. Bi, C.-R. Zhang, Q.-X. Luo, R.-P. Liang and J.-D. Qiu, Synergistic effect of photocatalytic

U(VI) reduction and chlorpyrifos degradation by bifunctional type-II heterojunction MOF525@BDMTp with high carrier migration performance, *Appl. Catal., B*, 2024, **342**, 123460.

8 M. Chen, T. Liu, X. Zhang, R. Zhang, S. Tang, Y. Yuan, Z. Xie, Y. Liu, H. Wang, K. V. Fedorovich and N. Wang, Photoinduced enhancement of uranium extraction from seawater by MOF/black phosphorus quantum dots heterojunction anchored on cellulose nanofiber aerogel, *Adv. Funct. Mater.*, 2021, **31**, 2100106.

9 X. Zhong, Y. Liu, W. Liang, Y. Zhu and B. Hu, Construction of core-shell MOFs@COF hybrids as a platform for the removal of UO_2^{2+} and Eu^{3+} ions from solution, *ACS Appl. Mater. Interfaces*, 2021, **13**, 13883–13895.

10 Q. Sun, B. Aguila, L. D. Earl, C. W. Abney, L. Wojtas, P. K. Thallapally and S. Ma, Covalent organic frameworks as a decorating platform for utilization and affinity enhancement of chelating sites for radionuclide sequestration, *Adv. Mater.*, 2018, **30**, 1705479.

11 H. Yang, M. Hao, Y. Xie, X. Liu, Y. Liu, Z. Chen, X. Wang, G. I. N. Waterhouse and S. Ma, Tuning local charge distribution in multicomponent covalent organic frameworks for dramatically enhanced photocatalytic uranium extraction, *Angew. Chem., Int. Ed.*, 2023, **62**, e202303129.

12 X. Zhong, Q. Ling, Z. Ren and B. Hu, Immobilization of U(VI) onto covalent organic frameworks with the different periodic structure by photocatalytic reduction, *Appl. Catal., B*, 2023, **326**, 122398.

13 W. R. Cui, C. R. Zhang, W. Jiang, F. F. Li, R. P. Liang, J. Liu and J. D. Qiu, Regenerable and stable sp^2 carbon-conjugated covalent organic frameworks for selective detection and extraction of uranium, *Nat. Commun.*, 2020, **11**, 436.

14 Y. Xie, Z. Li, C. Liu, Q. Song, Y. Liu, Z. Zhang and B. Han, Bipyridine-based conjugated microporous polymers for boosted photocatalytic U(VI) separation, *Chem. Commun.*, 2024, **60**, 13348–13351.

15 L. Chen, B. Chen, J. Kang, Z. Yan, Y. Jin, H. Yan, S. Chen and C. Xia, The synthesis of a novel conjugated microporous polymer and application on photocatalytic removal of uranium(VI) from wastewater under visible light, *Chem. Eng. J.*, 2022, **431**, 133222.

16 X. Wang, W. Xu and W.-R. Cui, Modulating conjugated microporous polymers via cyclization as a remarkable photo-enhanced uranium recovery platform, *J. Hazard. Mater.*, 2024, **463**, 132846.

17 M. Xu, T. Wang, P. Gao, L. Zhao, L. Zhou and D. Hua, Highly fluorescent conjugated microporous polymers for concurrent adsorption and detection of uranium, *J. Mater. Chem. A*, 2019, **7**, 11214–11222.

18 Z. Xu, S. Yu, J. Wang, F. Yu, M. Xu, J. Xiong, S. Xiao, Y. Liu, Y. He, J. Xu, Z. Zhang and J. Qiu, Synchronous construction of high sulfonic acid grafting degree and large surface area in conjugated microporous polymer adsorbents for efficient removal of uranium(VI), *Sep. Purif. Technol.*, 2023, **309**, 122953.

19 L. Wang, Y. Wan, Y. Ding, S. Wu, Y. Zhang, X. Zhang, G. Zhang, Y. Xiong, X. Wu, J. Yang and H. Xu, Conjugated microporous polymer nanosheets for overall water splitting using visible light, *Adv. Mater.*, 2017, **29**, 1702428.

20 J. M. Lee and A. I. Cooper, Advances in Conjugated Microporous Polymers, *Chem. Rev.*, 2020, **120**, 2171–2214.

21 F. Yu, Z. Zhu, S. Wang, J. Wang, Z. Xu, F. Song, Z. Dong and Z. Zhang, Novel donor-acceptor-acceptor ternary conjugated microporous polymers with boosting forward charge separation and suppressing backward charge recombination for photocatalytic reduction of uranium(VI), *Appl. Catal., B*, 2022, **301**, 120819.

22 A. Satpathy, J. G. Catalano and D. E. Giammar, Reduction of U(VI) on chemically reduced montmorillonite and surface complexation modeling of adsorbed U(IV), *Environ. Sci. Technol.*, 2022, **56**, 4111–4120.

23 R. Dawson, A. Laybourn, Y. Z. Khimyak, D. J. Adams and A. I. Cooper, High surface area conjugated microporous polymers: The importance of reaction solvent choice, *Macromolecules*, 2010, **43**, 8524–8530.

24 L. Zhang, N. Pu, B. Yu, G. Ye, J. Chen, S. Xu and S. Ma, Skeleton engineering of homocoupled conjugated microporous polymers for highly efficient uranium capture via synergistic coordination, *ACS Appl. Mater. Interfaces*, 2020, **12**, 3688–3696.

25 X. Qian, Z.-Q. Zhu, H.-X. Sun, F. Ren, P. Mu, W. Liang, L. Chen and A. Li, Capture and reversible storage of volatile iodine by novel conjugated microporous polymers dontaining thiophene units, *ACS Appl. Mater. Interfaces*, 2016, **8**, 21063–21069.

26 Y. B. Sun, S. H. Lu, X. X. Wang, C. Xu, J. X. Li, C. L. Chen, J. Chen, T. Hayat, A. Alsaedi, N. S. Alharbi and X. K. Wang, Plasma-facilitated synthesis of amidoxime/carbon nanofiber hybrids for effective enrichment of ^{238}U(VI) and ^{241}Am(III), *Environ. Sci. Technol.*, 2017, **51**, 12274–12282.

27 A. O. Mousa, M. G. Mohamed, Z.-I. Lin, C.-H. Chuang, C.-K. Chen and S.-W. Kuo, Construction of cationic conjugated microporous polymers containing pyrene units through post-cationic modification for enhanced antibacterial performance, *J. Taiwan Inst. Chem. Eng.*, 2024, **157**, 105448.

28 Y. Guo, Q.-M. Hasi, J. Yu, Y. Guo, L. Song, S. Wu, X. Luo and L. Chen, Carboxymethyl cellulose/sulfonated conjugated microporous polymer composite aerogel for efficient pollution removal and water evaporation, *Sep. Purif. Technol.*, 2023, **324**, 124518.

29 A. Yi, Y. Zhang, Q. Chen, C. Guo, J. J. H. Sun, R. Jiao, J. Li, Z. Zhu and A. Li, CMPs-based aerogels for dual-phase iodine capture: Gas and organic medium, *Sep. Purif. Technol.*, 2025, **376**, 134052.

30 Y. Sun, J. Xiao, X. Huang, P. Mei and H. Wang, Boosting photocatalytic efficiency of MoS_2/CdS by modulating morphology, *Environ. Sci. Pollut. Res.*, 2022, **29**, 73282–73291.

31 X. Cao, K. Yu, Y. Zhang, N. Li, P. Wang, L. Zhou, X. Gong, H. Wang, F. Yang, W. Zhu and R. He, Efficient strategy for U(VI) photoreduction: Simultaneous construction of U(VI) confinement sites and water oxidation sites, *ACS Appl. Mater. Interfaces*, 2023, **15**, 1063–1072.

32 Y. Yue, J. Xiao, W. Zhu, B. Zhang, R. Hou, A. Ishag and Y. Sun, Fabrication of $MoS_2/CdS/TiO_2$ composites for photoreduction of U(VI) under visible light, *Mater. Res. Bull.*, 2024, **176**, 112839.
33 P. Mei, J. Xiao, X. Huang, A. Ishag and Y. Sun, Enhanced photocatalytic reduction of U(VI) on $SrTiO_3/g\text{-}C_3N_4$ composites : Synergistic interaction, *Eur. J. Inorg. Chem.*, 2022, **2022**, e202101005.
34 X. Huang, J. Xiao, P. Mei, H. Wang, A. Ishag and Y. Sun, The synthesis of Z-scheme $MoS_2/g\text{-}C_3N_4$ heterojunction for enhanced visible-light-driven photoreduction of uranium, *Catal. Lett.*, 2022, **152**, 1981–1989.
35 Z. Dong, S. Hu, Z. Li, J. Xu, D. Gao, F. Yu, X. Li, X. Cao, Y. Wang, Z. Zhang, Y. Liu and X. Wang, Biomimetic photocatalytic system designed by spatially separated cocatalysts on Z-scheme heterojunction with identified charge-transfer processes for boosting removal of U(VI), *Small*, 2023, **19**, 2300003.
36 Y. Zhang, M. Zhu, S. Zhang, Y. Cai, Z. Lv, M. Fang, X. Tan and X. Wang, Highly efficient removal of U(VI) by the photoreduction of $SnO_2/CdCO_3/CdS$ nanocomposite under visible light irradiation, *Appl. Catal., B*, 2020, **279**, 119390.
37 F. He, Q. Xiao, Y. Chen, H. Wang and X. Wang, Synergistic reduction of U(VI) and selective oxidation of benzyl alcohol to prepare benzaldehyde via $WO_x/g\text{-}C_3N_4$, *Appl. Catal., B*, 2024, **343**, 123525.
38 S. Yang, Y. Cao, T. Wang, S. Cai, M. Xu, W. Lu and D. Hua, Positively charged conjugated microporous polymers with antibiofouling activity for ultrafast and highly selective uranium extraction from seawater, *Environ. Res.*, 2020, **183**, 109214.
39 Z. F. Li, Z. B. Zhang, Z. Q. Lin, K. Zhao, B. Han, S. Yao and Y. H. Liu, Recent advances of covalent organic frameworks-based materials for photocatalytic U(VI) separation: Structural modulation and mechanistic exploration, *ChemSusChem*, 2025, **18**, e202500972.